Published in final edited form as:
ACS Nano. 2018 January 23; 12(1): 89–94. doi:10.1021/acsnano.7b07496.

Charge-switchable nanozymes for bioorthogonal imaging of biofilm-associated infections

Akash Gupta[‡,†], **Riddha Das**[‡,†], **Gulen Yesilbag Tonga**[‡], **Tsukasa Mizuhara**[‡], and **Vincent M. Rotello**[‡,*]

[‡]Department of Chemistry, University of Massachusetts Amherst, 710 North Pleasant Street, Amherst, Massachusetts 01003, United States

Abstract

Early detection of biofilms is crucial for limiting infection-based damage. Imaging these biofilms is challenging: conventional imaging agents are unable to penetrate the dense matrix of the biofilm, and many imaging agents are susceptible to false positive/negative responses due to phenotypical mutations of the constituent microbes. We report the creation of pH-responsive nanoparticles with embedded transition metal catalysts (nanozymes) that effectively target the acidic microenvironment of biofilms. These pH-switchable nanozymes generate imaging agents through bio-orthogonal activation of pro-fluorophores inside biofilms. The specificity of these nanozymes for imaging biofilms in complex biosystems was demonstrated using co-culture experiments.

Graphical Abstract

---

[*] Corresponding Author: rotello@chem.umass.edu.

[†] **Author Contributions**
Akash Gupta and Riddha Das contributed equally.

The authors declare no competing financial interests.

Supporting information for this manuscript contains: synthesis and characterization of gold nanoparticles, quantification of Au and Ru using ICP-MS, nanozymes catalysis in solution, confocal imaging of 4 different strains of biofilms, imaging of mammalian cells, data analysis of confocal images.

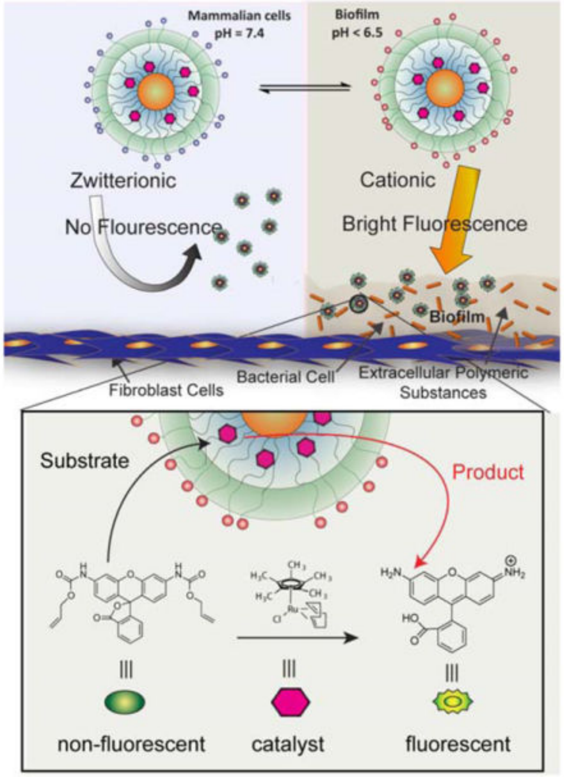

Keywords

Biofilms; extracellular polymeric substance; pH-responsive; nanoparticles; nanozymes

---

Bacterial infections are serious threat to public health, causing > 2 million cases of illnesses and >23,000 deaths each year in U.S.[1] The majority of human bacterial infections (~80%) are associated with biofilm formation on living tissues.[2] Biofilms are three-dimensional bacterial communities where microbes reside in an extracellular polymeric substance (EPS) matrix, and are highly protected from exogenous agents. Biofilm-associated infections are responsible for a range of chronic diseases including endocarditis, osteomyelitis and implant dysfunction, and are key co-morbity threats for other diseases such as cystic fibrosis.[3,4] Currently, biofilm infections are typically diagnosed only after they have become systemic or have caused significant anatomical damage,[5,6] highlighting the need for effective imaging tools.

Current techniques for imaging bacteria use probes such as autologous white blood cells[7], maltodextrin[8] and dipicolylamine zinc (II).[9] Although these systems are effective for imaging planktonic (dispersed) bacterial infections, only limited studies have been conducted on imaging of biofilm-associated infections.[10,11,12] Other imaging modalities such as ^{67}Ga-citrate and radiolabeled autologous white blood cells lack the spatial resolution required for surgical procedures such as debridement of infected tissue.[6,13] Most high resolution optical imaging approaches rely on fluorescent dyes conjugated to a biorecognition element, generating highly specific imaging probes that are susceptible to false responses due to phenotypic mutations of biofilm residing microbes.[14,15] Moreover, physical heterogeneity and complex biofilm architecture further complicates imaging of these highly refractory infections.[16] In particular, the dense and amphiphilic nature of EPS matrix prevents the penetration of imaging agents.[17,18] Synthetic macromolecules such as nanoparticles (NPs) have shown potential to penetrate biofilms[19], however they currently lack the ability to intrinsically target these resilient infections.[20,21]

Biofilms have inherently acidic microenvironments (pH 4.5–6.5) as a by-product of sugar fermentation caused by bacteria.[22] For instance, pH in human dental biofilms often reaches below 4.5 causing acidic dissolution of tooth enamel.[23] Similarly, cystic fibrosis (CF) pulmonary infections are associated with acidification of airways in CF patients.[24] We hypothesized that pH-responsive sulfonamide-functionalized gold nanoparticles (AuNPs)[25] could be used to target this acidic environment. In this system, targeting of the biofilm is achieved through charge-switchable NPs that transition from zwitterionic (non-adhesive) to cationic (adhesive) at the pH values typically found in biofilms, providing a broad-spectrum recognition platform for bacteria with selectivity towards biofilms compared to healthy mammalian cells. Imaging of the biofilms is achieved by the embedded transition metal catalysts (TMCs) that activate the pro-fluorophores *in situ* inside the biofilms. These bioorthogonal 'nanozymes' provide an effective imaging system that selectively targets bacterial biofilms and provides amplified fluorescence signal output using bioorthogonal catalysis. This nanozyme platform was used to effectively image biofilms of different bacterial species with complete EPS matrix penetration, and to image biofilms in a complex mammalian cell - biofilm co-culture model.

RESULTS AND DISCUSSIONS

Sensing was performed with 2nm AuNPs featuring terminal groups with distinct pK_a values to selectively target the acidic microenvironment of biofilms.[25] Alkoxyphenyl acylsulfonamide-functionalized **NP1** features groups that are protonated under weakly acidic conditions ($pK_a \sim 6.5$), consistent with normal biofilm pH. Acylsulfonamide-functionalized NP2 has slightly lower pK_a (~4.5) than its aryl analog, providing a tool for measuring the lower extremes of biofilm pH. Finally, **NP3** features a sulfobetaine termini, providing a stable zwitterionic control for our studies ($pKa < 1$) (Figure 1a).[26,27] These particles were synthesized from pentane-thiol capped 2nm core AuNPs using a place exchange reaction (synthesis and characterization of NPs is described in supporting information, SI Figure S1).

The nanozymes were generated through encapsulation of a ruthenium-based catalyst- [Cp*Ru(cod)Cl] (Cp* = pentamethylcyclopentadienyl, cod = 1,5-cyclooctadiene) into the ligand monolayer of **NP1-3** to generate the respective nanozymes (**NZ1-3**).[28] Transmission electron microscopy (TEM) images and dynamic light scattering data of NPs before and after encapsulation of catalysts show no signs of aggregation (SI Figure S2 and S3). Further size distribution studies for NZs were conducted at a range of pH (3.5–7.4) using DLS, demonstrating their stability even in the acidic conditions (SI Figure S4). The quantification of catalysts encapsulated was done using inductively-coupled plasma mass spectrometry (ICP-MS, SI Figure S6), indicating that 24 ± 2 catalyst molecules were encapsulated per

AuNP for **NZ1-3**. The catalysts encapsulated per AuNP were similar at different pH ranges (3.5–7.4), as validated using ICP-MS (SI, Table S1).

The catalytic activities of **NZ1-3** were assessed in solution by deallylation of bis-N, N′-allyloxycarbonyl rhodamine 110 (**alloc-Rho**, Figure 1) at pH = 7.4.[29] The rate of increase in fluorescence was similar (Figure 2a) for the **NZ1-3** complexes, indicating similar catalytic activity for all NZs at physiological pH. Further, we tested the catalytic activity of **NZ1** with varying pH (3.5–7.4), indicating no significant difference in the catalysis rate for the nanozyme (SI, Figure S8).

After establishing their catalytic activity in solution, we determined the pH dependence of the NZ's surface charge by measuring their zeta potential. The surface charge of all three **NZs (1-3)** were close to neutral at physiological pH (7.4), consistent with their zwitterionic structures. **NZ (1-2)** exhibited a sharp transition from neutral to overall positive charge at pH 6.5 and pH 4.5 respectively, consistent with their respective pKa's. As expected, **NZ3** possessed near neutral charge even at highly acidic pH values as seen in Figure 2b and SI Figure S5. Next, we performed NZ diffusion studies in biofilms using ICP-MS to investigate their ability to penetrate and accumulate inside biofilms. We observed that switchable **NZ1** showed the highest diffusion into biofilms based on Au, with lesser amounts observed with **NZ2** and **NZ3** respectively (Figure 2c). This trend is mirrored in the Ru signal from the catalyst. This overall change to cationic surface charge of the pH-responsive NZs can play a crucial role in their ability to intrinsically target biofilms over the mammalian cells (SI, Figure S9).

We then investigated the ability of NZs to image biofilms using confocal microscopy. We chose uropathogenic clinical isolate of *P. aeruginosa* (CD-1006) as a model strain for imaging studies due to their high prevalence in clinical biofilms.[30,31] Imaging studies of biofilms were based on generation of fluorophore (Rhodamine 110) through deallylation of a non-fluorescent precursor as shown in Figure 1b. Catalytic activity of the NZs was probed inside the biofilms by incubating the NZs with biofilms for 1 h, followed by multiple washings to remove absorbed particles. Fresh media containing substrate was added following 1 h incubation and subsequent washings. Confocal images of biofilms treated with switchable **NZ1** exhibited bright fluorescence, with only localized fluorescence observed with **NZ2**, and little or no fluorescence beyond auto fluorescence observed with **NZ3**, results mirrored in the quantified intensities (Figure 2d, e). Additionally, mammalian cells treated with charge switchable nanozymes exhibited minimal fluorescence after incubation of 3 hours (SI Figure S12). These results suggest that pH responsive zwitterionic nanozyme **NZ1** can be used to target the biofilms for imaging applications.

Z-stack confocal imaging was used to determine the localization of activated fluorophores inside DS Red (red fluorescent protein) expressing *E. coli* biofilms (Figure 3a). The penetration profile of **NZ1** was quantified by using NIS element analysis software.[32] The intensity of green and red channel represents the intensity of Rhodamine-110 and biofilms respectively. The integrated intensities were normalized at the top layer of biofilm to compare their co-localization with varying biofilm depth (0–5.6 μm). As shown in Figure 3b, the activated fluorophore (Rhodamine 110) was distributed throughout the biofilm.

Biofilms incubated without **NZ1** were used as negative control (SI Figure S11). The ability of switchable **NZ1** to image bacterial biofilms was further validated against three bacterial strains of clinical isolates - *Enterobacter cloacae* (CD-1412), methicillin-resistant *Staphylococcus aureus* (CD-489) and *Escherichia coli* (CD-2), demonstrating effective imaging of biofilms formed by both Gram positive (*S. aureus*) and Gram negative (*E. coli, P. aeruginosa, E. cloacae*) (SI Figure S10) species. Further, we tested the cytotoxicity of these NZs against NIH 3T3 Fibroblast-cells that maintain high cell viability at 2 μM NZ incubation (Figure 3c). These studies indicate the biocompatibility of our zwitterionic nanozymes with mammalian cells.

Imaging of biofilms on biomedical surfaces such as medical implants and indwelling devices is a critical capability. However, tracking biofilm-associated infections on human tissues and organs is even more challenging and relevant for medical applications. In most cases of bacterial infections, microbes are embedded in human tissues inside resilient biofilms comprised of EPS.[33] Having established that pH responsive **NZ1** exhibits the highest selectivity towards biofilms and are non-toxic to fibroblast cells, we next investigated their ability to track biofilms, using fibroblast-biofilm co-culture as a model. We chose DS Red (red fluorescent protein) expressing *E. coli* as representative strain to generate co-culture model using previously established protocols.[34,35,36] Co-cultures were then incubated with **NZ1** for 1 hour, followed by multiple washings to remove non-adhering NZs. Subsequently, substrate **alloc-Rho** was added in fresh media for 1 hour, followed by multiple washing to remove excess substrate. The co-culture models were examined using confocal microscopy, exhibiting strong co-localization of Rhodamine and DS Red (from biofilm) and minimal fluorescence around mammalian cells (Figure 4, procedure to analyze image intensity is described in Supporting Information). The co-cultures incubated with alloc-Rho in absence of **NZ1** was used as negative control (SI, Figure S12). This high level of selectivity demonstrates the potential of switchable NZs to image bacterial biofilms in physiologically relevant conditions. Their ability to selectively target the biofilms can be attributed to the overall change in their surface charge (from neutral to cationic) at acidic conditions. The positively charged **NZ1** shows high accumulation inside the biofilm, whereas the neutral charged **NZ1** exhibits minimal uptake in fibroblast cells. Hence, the pro-fluorophore gets selectively activated in the biofilm, already inhabited by the charge switchable nanozyme.

CONCLUSION

In conclusion, we have developed a strategy for rapid and effective imaging of biofilms that was effective in a complex co-culture model. The pH-responsive NPs penetrate and accumulate inside the acidic microenvironment of biofilms, with bioorthogonal catalysis providing a sensitive readout mechanism. This bioorthogonal activation of imaging agents is a promising approach to detect biofilm-associated infections, and to locate infected sites during critical debridement surgeries. These pH responsive nanozymes offer a broad-spectrum strategy for imaging biofilms arising from different and/or mixed bacteria species, circumventing the need for designing microbe-specific probes. Considering their enhanced ability to penetrate the biofilm matrix, nanozymes hold a strong advantage against currently used imaging probes. In a broader context, this study demonstrates the utility of bioorthogonal catalysis for bioimaging.

Materials and Methods

All chemicals and solvents for synthesis were purchased from Fisher Scientific and Sigma-Aldrich, and used without further purification, unless otherwise stated. NIH-3T3 cells (ATCC CRL-1658) were purchased from ATCC. Dulbecco's Modified Eagle's Medium (DMEM) (DMEM; ATCC 30-2002) and fetal bovine serum (Fisher Scientific, SH3007103) were used in cell culture.

Synthesis and characterization of AuNPs

Detailed procedure of ligand and nanoparticle synthesis is described in the supporting information.

Catalyst encapsulation in AuNP monolayer

The catalyst, [Cp*Ru(cod)Cl] (3.0 mg) was dissolved in 1 ml acetone and the AuNP (20 μM, 0.5 mL) were diluted to a final concentration of 5 μM with DI water (1 ml). Then, the catalyst and the AuNP solutions were mixed together and acetone was slowly removed by evaporation. During the evaporation, hydrophobic catalyst was encapsulated in the particle monolayer to yield to NP_Ru. Excess catalysts which precipitated in water were removed by filtration (Millex-GP filter; 25 mm PES, pore Size: 0.22μm) and dialysis (Snake Skin® dialysis tubing, 10K) against water (5 L) for 24 h. Further purifications were followed by multiple filtrations (five times, Amicon® ultra 4, 10K) to remove free catalysts. The amount of encapsulated catalysts was measured by ICP-MS by tracking ^{101}Ru relative to ^{197}Au for NP_Ru.

Nanozyme kinetics in solution

Allylcarbamate protected Rhodamine 110 (**alloc-Rho**) was used as a substrate to test the catalytic activity of the nanozymes. A solution containing 100 nM nanozyme and 1 μM substrate was prepared in a 96-well plate. 400 nM nanozyme solution and 100 μM substrate solutions alone were used as negative controls. The kinetic study was done by tracking the fluorescence intensity (Ex: 488 nm, Em: 521 nm, Cutoff: 515 nm) using a Molecular Devices SpectraMax M2 microplate reader.

Biofilm culture

Bacteria were inoculated in LB broth at 37°C until stationary phase. The cultures were then harvested by centrifugation and washed with 0.85% sodium chloride solution three times. Concentrations of resuspended bacterial solution were determined by optical density measured at 600 nm. Seeding solutions were then made in minimal media, M9 broth to reach OD_{600} of 0.1. 500 μL of the seeding solutions were added to each well of the 24-well microplate. M9 medium without bacteria was used as a negative control. The plates were covered and incubated at room temperature under static conditions for a desired period of 24 hours. Planktonic bacteria were removed by washing with PB saline three times.

Diffusion of nanozymes inside biofilms

After plating bacterial cells in a 24-well plate. On the following day, planktonic bacteria were removed by washing with PBS three times. and incubated with **NZ 1**, **NZ 2** and **NZ 3** (400 nM each) in minimal M-9 media (pH 7.4) for 3 h at 37 °C. After incubation, biofilms were washed three times with PBS and lysis buffer was added to each well. All lysed samples were then further processed for ICP-MS analysis (*vide infra*) to determine the intracellular amount of gold and ruthenium. Diffusion experiments were performed independently at least two times and each experiment was comprised of three replicates.

Confocal imaging of biofilms

10^8 bacterial cells/ml were seeded (2 ml in M9 media) in a confocal dish and were allowed to grow, old media was replaced every 24 hours. After 3 days media was replaced by 400 nM of the **NZ 1, NZ 2 and NZ 3** and biofilms were incubated for 1 h, biofilm samples incubated with only M9 media were used as control. After 1 h, biofilms were washed with PBS three times and were incubated with 100 μM of the substrates for 1 h. The cells were then washed with PBS three times. Confocal microscopy images were obtained on a Zeiss LSM 510 Meta microscope by using a 60× objective. The settings of the confocal microscope were as follows: green channel: λ_{ex}=488 nm and λ_{em}=BP 505–530 nm; red channel: λ_{ex}=543 nm and λ_{em}=LP 650 nm. Emission filters: BP=band pass, LP=high pass.

Mammalian cell viability studies

These experiments were done using previously reported protocol.[37] Briefly, 20,000 NIH 3T3 fibroblast cells (ATCC CRL-1658) were cultured in DMEM medium in presence of 10% bovine calf serum and 1% antibiotic solution. The cells were cultured at 37 °C in a humidified atmosphere of 5% CO_2 for 48 h. Next, the cells were washed with phosphate-buffered saline (PBS) and different concentration of **NZs (1-3)** in 10% serum containing media were incubated with the cells for 3 h at 37 °C. After the incubation period, cells were washed with PBS (3 times) and cell viability was then determined using Alamar blue assays according to manufacturer's protocol (Invitrogen Biosource). Washed cells were incubated with 220 μl of 10% Alamar Blue solution in 10% serum containing media. The solution was incubated at 37 °C under a humidified atmosphere of 5% CO_2 for 3 h. Subsequently, 200 μl solution from the wells was transferred in a 96-well black-microplate. The fluorescence reading was measured using a UV/vis spectrophotometer with excitation and emission at 560 and 590 nm respectively. Cell incubated without NPs were treated as 100% viable cells and the cell viability was calculated accordingly. These experiments were performed in triplicates.

Imaging of Co-culture models

Fibroblast-3T3 co-culture was performed using a previously reported protocol.[36] A total of 20,000 NIH 3T3 (ATCC CRL-1658) cells were cultured in Dulbecco's modified Eagle medium (DMEM; ATCC 30-2002) with 10% bovine calf serum and 1% antibiotics at 37°C in a humidified atmosphere of 5% CO_2. Cells were kept for 24 hours to reach a confluent monolayer in a confocal dish. Bacteria (*P. aeruginosa*) were inoculated and harvested as mentioned above. Afterwards, seeding solutions 10^8 cells/ml were inoculated in buffered

DMEM supplemented with glucose. Old media was removed from 3T3 cells followed by addition of 2 mL of seeding solution. The co-cultures were then stored in a box humidified with damp paper towels at 37°C overnight without shaking. The co-cultures were treated with NZs and substrates using similar procedure used for biofilm models.

Supplementary Material

Refer to Web version on PubMed Central for supplementary material.

Acknowledgments

Funding Sources

This research was supported by the NIH (EB022641 and GM077173) and NSF (CHE-1506725).

Clinical samples obtained from the Cooley Dickinson Hospital Microbiology Laboratory (Northampton, MA) were kindly provided by Dr. Margaret Riley.

References

1. FY15 Detect and Protect Against Antibiotic Resistance Budget Initiative. Centers for Disease Control and Prevention; Atlanta, GA: 2003. http://www.cdc.gov/drugresistance/threat-report-2013/pdf/FY15-DPAR-budget-init.pdf
2. Lewis K. Persister Cells, Dormancy and Infectious Disease. Nat Rev Micro. 2007; 5:48–56.
3. Hall-Stoodley L, Costerton JW, Stoodley P. Bacterial Biofilms: From the Natural Environment to Infectious Diseases. Nat Rev Microbiol. 2004; 2:95–108. [PubMed: 15040259]
4. Bjarnsholt T. The Role of Bacterial Biofilms in Chronic Infections. Apmis. 2013; 121:1–58. [PubMed: 23030626]
5. Costerton JW, Post JC, Ehrlich GD, Hu FZ, Kreft R, Nistico L, Kathju S, Stoodley P, Hall-Stoodley L, Maale G, James G, Sotereanos N, DeMeo P. New Methods for the Detection of Orthopedic and Other Biofilm Infections. FEMS Immunol Med Microbiol. 2011; 61:133–140. [PubMed: 21204998]
6. van Oosten M, Schäfer T, Gazendam JAC, Ohlsen K, Tsompanidou E, de Goffau MC, Harmsen HJM, Crane LMA, Lim E, Francis KP, Cheung L, Olive M, Ntziachristos V, Dijl JMV, Dam GMV. Real-Time *in vivo* Imaging of Invasive- and Biomaterial-Associated Bacterial Infections Using Fluorescently Labelled Vancomycin. Nat Commun. 2013; 4:2584. [PubMed: 24129412]
7. Love C, Tomas MB, Tronco GG, Palestro CJ. FDG PET of Infection and Inflammation. Radiographics. 2005; 25:1357–1368. [PubMed: 16160116]
8. Ning X, Lee S, Wang Z, Kim D, Stubblefield B, Gilbert E, Murthy N. Maltodextrin-Based Imaging Probes Detect Bacteria *in vivo* with High Sensitivity and Specificity. Nat Mater. 2011; 10:602–607. [PubMed: 21765397]
9. Leevy WM, Gammon ST, Jiang H, Johnson JR, Maxwell DJ, Jackson EN, Marquez M, Piwnica-Worms D, Smith BD. Optical Imaging of Bacterial Infection in Living Mice Using a Fluorescent near-Infrared Molecular Probe. J Am Chem Soc. 2006; 128:16476–16477. [PubMed: 17177377]
10. Hall-Stoodley L, Stoodley P, Kathju S, Høiby N, Moser C, William Costerton J, Moter A, Bjarnsholt T. Towards Diagnostic Guidelines for Biofilm-Associated Infections. FEMS Immunol Med Microbiol. 2012; 65:127–145. [PubMed: 22469292]
11. Sauer K, Camper AK, Ehrlich GD, Costerton JW, Davies DG. Pseudomonas Aeruginosa Displays Multiple Phenotypes during Development as a Biofilm. J Bacteriol. 2002; 184:1140–1154. [PubMed: 11807075]
12. Hall-Stoodley L, Hu FZ, Gieseke A, Nistico L, Nguyen D, Hayes J, Forbes M, Greenberg DP, Dice B, Burrows A, Wackym PA, Stoodley P, Post JC, Ehrlich GD, Kerschner JE. Direct Detection of Bacterial Biofilms on the Middle-Ear Mucosa of Children with Chronic Otitis Media. J Am Med Assoc. 2006; 296:202–211.

13. Sasser TA, Avermaete AE, Van White A, Chapman S, Johnson JR, Avermaete T, Van Gammon ST, Leevy WM, Health C, Imaging M. Bacterial Infection Probes and Imaging Strategies in Clinical Nuclear Medicine and Preclinical Molecular Imaging. Curr Top Med Chem. 2013; 13:479–487. [PubMed: 23432010]
14. Neu TR, Swerhone GDW, Lawrence JR. Assessment of Lectin-Binding Analysis for *in situ* Detection of Glycoconjugates in Biofilm Systems. Microbiology. 2001; 147:299–313. [PubMed: 11158347]
15. Bjarnsholt T, Alhede M, Alhede M, Eickhardt-Sørensen SR, Moser C, Kühl M, Jensen PØ, Høiby N. The *in vivo* Biofilm. Trends Microbiol. 2013; 21:466–474. [PubMed: 23827084]
16. Fux, Ca, Stoodley, P., Hall-Stoodley, L., Costerton, JW. Bacterial Biofilms: A Diagnostic and Therapeutic Challenge. Expert Rev Anti Infect Ther. 2003; 1:667–683. [PubMed: 15482163]
17. Anderl JN, Franklin MJ, Stewart PS. Role of Antibiotic Penetration Limitation in Klebsiella Pneumoniae Biofilm Resistance to Ampicillin and Ciprofloxacin. Antimicrob Agents Chemother. 2000; 44:1818–1824. [PubMed: 10858336]
18. Stewart PS, Costerton JW. Antibiotic Resistance of Bacteria in Biofilms. Lancet. 2001; 358:135–138. [PubMed: 11463434]
19. Li X, Yeh YC, Giri K, Mout R, Landis RF, Prakash YS, Rotello VM. Control of Nanoparticle Penetration into Biofilms through Surface Design. Chem Commun. 2015; 51:282–285.
20. Peulen TO, Wilkinson KJ. Diffusion of Nanoparticles in a Biofilm. Environ Sci Technol. 2011; 45:3367–3373. [PubMed: 21434601]
21. Gupta A, Landis RF, Rotello VM. Nanoparticle-Based Antimicrobials: Surface Functionality Is Critical. F1000Research. 2016; 5:1–10.
22. Benoit DSW, Koo H. Targeted, Triggered Drug Delivery to Tumor and Biofilm Microenvironments. Nanomedicine. 2016; 11:873–879. [PubMed: 26987892]
23. Horev B, Klein MI, Hwang G, Li Y, Kim D, Koo H, Benoit DSW. PH-Activated Nanoparticles for Controlled Topical Delivery of Farnesol to Disrupt Oral Biofilm Virulence. ACS Nano. 2015; 9:2390–2404. [PubMed: 25661192]
24. Moriarty TF, Elborn JS, Tunney MM. Effect of pH on the Antimicrobial Susceptibility of Planktonic and Biofilm-Grown Clinical Pseudomonas Aeruginosa Isolates. Br J Biomed Sci. 2007; 64:101–104. [PubMed: 17910277]
25. Mizuhara T, Saha K, Moyano DF, Kim CS, Yan B, Kim YK, Rotello VM. Acylsulfonamide-Functionalized Zwitterionic Gold Nanoparticles for Enhanced Cellular Uptake at Tumor pH. Angew Chemie - Int Ed. 2015; 54:6567–6570.
26. Das M, Sanson N, Kumacheva E. Zwitterionic Poly(betaine-N-Isopropylacrylamide) Microgels: Properties and Applications. Chem Mater. 2008; 20:7157–7163.
27. Madura JD, Lombardini JB, Briggs JM, Minor DL, Wierzbicki A. Physical and Structural Properties of Taurine and Taurine Analogues. Amino Acids. 1997; 13:131–139.
28. Tonga GY, Jeong Y, Duncan B, Mizuhara T, Mout R, Das R, Kim ST, Yeh YC, Yan B, Hou S, Rotello VM. Supramolecular Regulation of Bioorthogonal Catalysis in Cells Using Nanoparticle-Embedded Transition Metal Catalysts. Nat Chem. 2015; 7:597–603. [PubMed: 26100809]
29. Yusop RM, Unciti-Broceta A, Johansson EM, Sanchez-Martin RM, Bradley M. Palladium-Mediated Intracellular Chemistry. Nat Chem. 2011; 3:239–243. [PubMed: 21336331]
30. Oliver A, Canton R, Campo P, Baquero F, Blazquez J, Cantón R, Campo P, Baquero F, Blázquez J. High Frequency of Hypermutable Pseudomonas Aeruginosa in Cystic Fibrosis Lung Infection. Science. 2000; 288:1251–1253. [PubMed: 10818002]
31. Nickel JC, Ruseska I, Wright JB, Costerton JW. Tobramycin Resistance of Pseudomonas Aeruginosa Cells Growing as a Biofilm on Urinary Catheter Material. Antimicrob Agents Chemother. 1985; 27:619–624. [PubMed: 3923925]
32. Yun SW, Leong C, Zhai D, Tan YL, Lim L, Bi X, Lee JJ, Kim HJ, Kang NY, Ng SH, Stanton LW, Chang YT. Neural Stem Cell Specific Fluorescent Chemical Probe Binding to FABP7. Proc Natl Acad Sci. 2012; 109:10214–10217. [PubMed: 22689954]
33. Costerton W, Veeh R, Shirtliff M, Pasmore M, Post C, Ehrlich G. The Application of Biofilm Science to the Study and Control of Chronic Bacterial Infections. J Clin Invest. 2003; 112:1466–1477. [PubMed: 14617746]

34. Anderson GG, Moreau-Marquis S, Stanton BA, O'Toole GA. *In Vitro* Analysis of Tobramycin-Treated Pseudomonas Aeruginosa Biofilms on Cystic Fibrosis-Derived Airway Epithelial Cells. Infect Immun. 2008; 76:1423–1433. [PubMed: 18212077]

35. Anderson GG, Kenney TF, Macleod DL, Henig NR, O'Toole GA. Eradication of Pseudomonas Aeruginosa Biofilms on Cultured Airway Cells by a Fosfomycin/tobramycin Antibiotic Combination. Pathog Dis. 2013; 67:39–45. [PubMed: 23620118]

36. Landis RF, Gupta A, Lee Y-W, Wang L-S, Golba B, Couillaud B, Ridolfo R, Das R, Rotello VM. Crosslinked Polymer-Stabilized Nanocomposites for the Treatment of Bacterial Biofilms. ACS Nano. 2016; 11 acsnano.6b07537.

37. Gupta A, Saleh NM, Das R, Landis RF, Bigdeli A, Motamedchaboki K, Rosa Campos A, Pomeroy K, Mahmoudi M, Rotello VM. Synergistic Antimicrobial Therapy Using Nanoparticles and Antibiotics for the Treatment of Multidrug-Resistant Bacterial Infection. Nano Futur. 2017; 1:15004.

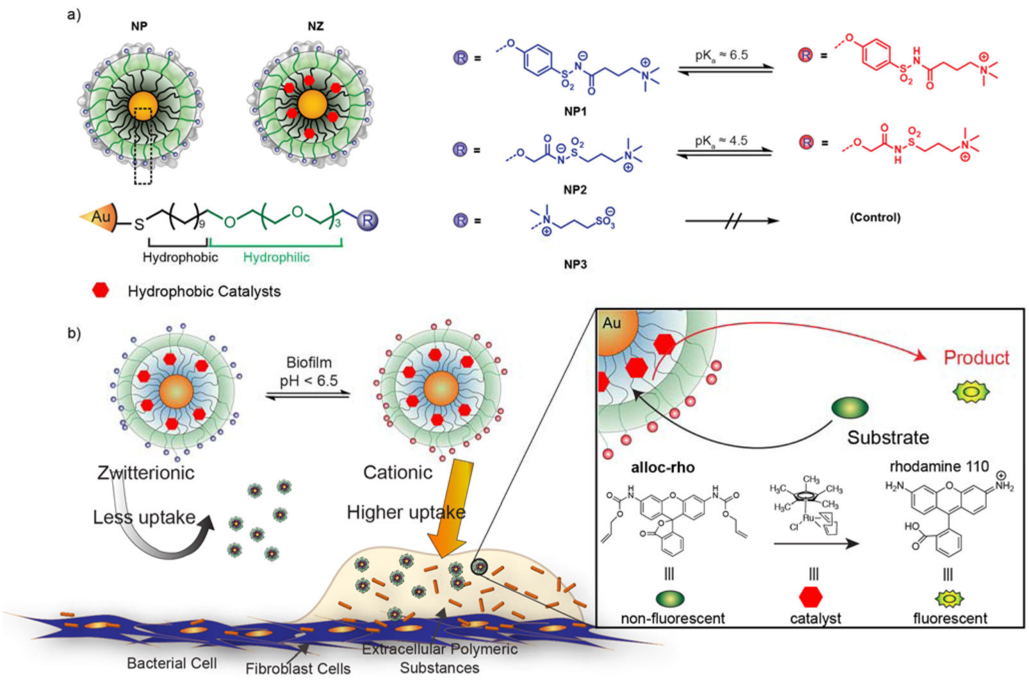

Figure 1.

a) Molecular structures of pH switchable and control ligands on gold nanoparticles (AuNPs). b) Schematic representation showing selective targeting of biofilm infections using pH responsive nanoparticles and intra-biofilm fluorogenesis of pro-fluorophores by transition metal catalysts (TMCs) embedded in the nanoparticle monolayers.

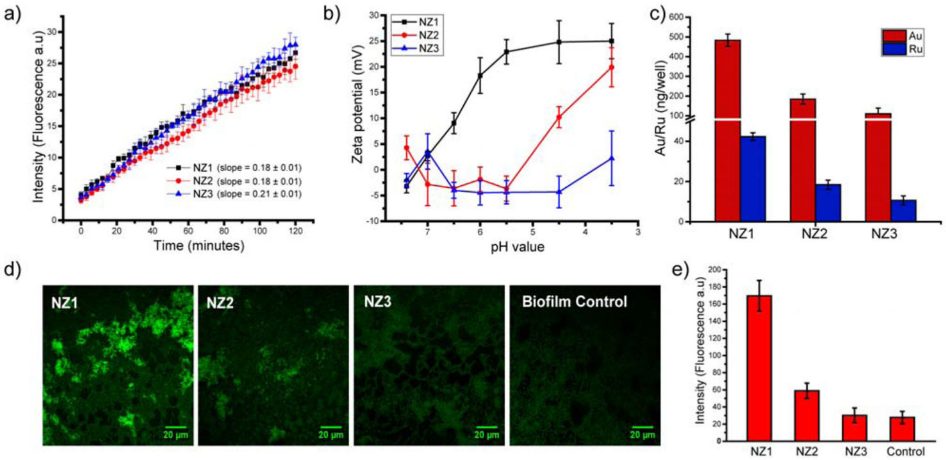

Figure 2.

a) Catalysis of nanozymes with different chemical headgroups in neutral pH for 2 hours at 37 ºC. b) Zeta potential of **NZ1-3** (1 μM) measured at range of pH (3.5–7.4) is plotted against different pH values. Error bars represent standard deviations based on three independent measurements per pH value. c) Nanoparticle and catalyst diffusion into *P. aeruginosa* (CD-1006) biofilms after incubation for 1 hour in pH 7.4 media with **NZ 1-3** (400 nM), as measured by ICP-MS. d) Confocal images of biofilm incubated with nanozymes (1-hour, 400 nM) followed by incubation with **alloc-Rho** (1 hour, 100 μM), Biofilm control is the negative control in absence of nanozyme. e) Quantitative analysis of fluorescence intensity generated upon addition of different nanozymes.

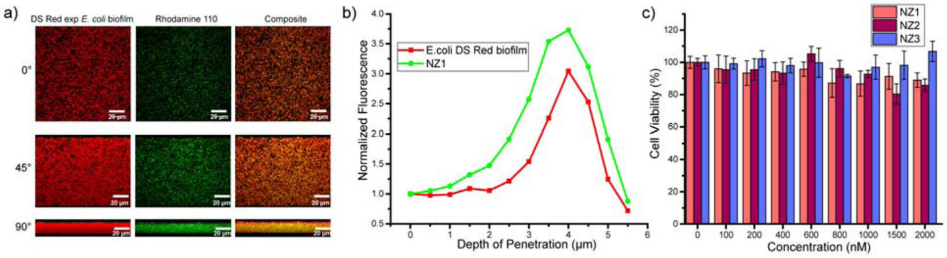

Figure 3.

a) Confocal microscopy images of DS Red exp *E. coli* and activated Rhodamine 110 fluorophore in presence of **NZ1**. Composite images show homogeneous co-localization of biofilm and activated fluorophores. The panels are projections at 0º, 45º and 90º angle turning along Y-axis. The scale bars are 20 µm. b) Integrated intensity of Rhodamine 110 and DS Red biofilm after 1-hour incubation with **NZ1**. The x-axis is the depth of penetration of biofilms, where 0 µm represents the top layer and ~5.6 µm, the bottom layer. The y-axis, normalized fluorescence, is normalized intensity of red and green channel at the top layer to compare their localization. c) Cell viability of 3T3-Fibroblast cells after 24-hour incubation with **NZ1-3** (0.1–2 µM). The data are average of triplicates and the error bars indicate standard deviations.

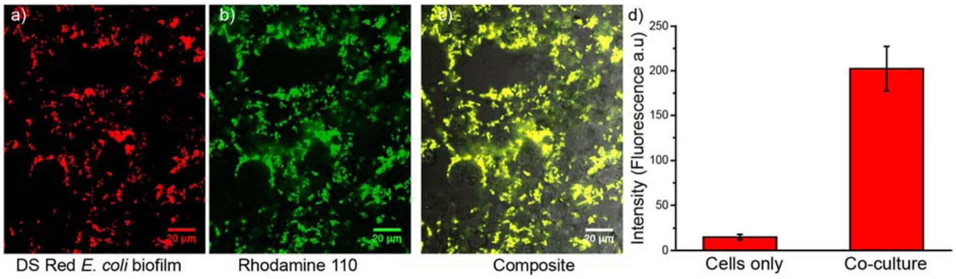

Figure 4.

Confocal images of a fibroblast-DS Red *E. coli* biofilm co-culture model incubated with switchable nanozyme **NZ1** (400 nM) and alloc-rhodamine (non-fluorescent, 100 µM) for 1 h. a) DS Red b) Rhodamine 110 and c) merged channels d) Quantitative analysis of fluorescence intensity observed in the images of non-infected cells (cells only) and cells infected with biofilm (co-culture). Scale bar is 20 µm.